Front. Mater. Sci. 2016, 10(3): 281–289
DOI 10.1007/s11706-016-0345-9

RESEARCH ARTICLE

Blood compatibility of zinc–calcium phosphate conversion coating on Mg–1.33Li–0.6Ca alloy

Yu-Hong ZOU[1], Rong-Chang ZENG (✉)[2,4], Qing-Zhao WANG[1], Li-Jun LIU[2], Qian-Qian XU[3], Chuang WANG[1], and Zhi-Wei LIU[1]

1 College of Chemical and Environmental Engineering, Shandong University of Science and Technology, Qingdao 266590, China
2 College of Materials Science and Engineering, Shandong University of Science and Technology, Qingdao 266590, China
3 Hospital of Shandong University of Science and Technology, Qingdao 266590, China
4 State Key Laboratory of Mining Disaster Prevention and Control Co-founded by Shandong Province and the Ministry of Science and Technology, Shandong University of Science and Technology, Qingdao 266590, China

ABSTRACT: Magnesium alloys as a new class of biomaterials possess biodegradability and biocompatibility in comparison with currently used metal implants. However, their rapid corrosion rates are necessary to be manipulated by appropriate coatings. In this paper, a new attempt was used to develop a zinc–calcium phosphate (Zn–Ca–P) conversion coating on Mg–1.33Li–0.6Ca alloys to increase the biocompatibility and improve the corrosion resistance. *In vitro* blood biocompatibility of the alloy with and without the Zn–Ca–P coating was investigated to determine its suitability as a degradable medical biomaterial. Blood biocompatibility was assessed from the hemolysis test, the dynamic cruor time test, blood cell count and SEM observation of the platelet adhesion to membrane surface. The results showed that the Zn–Ca–P coating on Mg–1.33Li–0.6Ca alloys had good blood compatibility, which is in accordance with the requirements for medical biomaterials.

KEYWORDS: magnesium alloy; lithium; biomaterial; biocompatibility; zinc–calcium phosphate coating

Contents

Received April 5, 2016; accepted May 20, 2016

E-mail: rczeng@foxmail.com

1 Introduction

Mg-based alloys have attracted increasing attention as newest biodegradable metal materials and have been widely researched in recent years [1–4]. Magnesium as a necessary element in the human body has many functions in bone growth, muscle contraction, inhibition of abnormal nerve excitability and temperature regulation as well as maintaining the stability of the structure of nucleic acid and participating in the body protein synthesis [5]. In addition, magnesium plays a critical role in stabilization of membrane potential and regulation of cellular excitability [6]. The human body is known to contain as much as 30 g of magnesium, the majority of which is mostly stored in bone, muscle, and other soft tissues. The released magnesium ions are either stored in fracture callus and new bone or eliminated into blood circulation and excreted by urine without causing remarkable incidence of hypermagnesium after its implantation [7–8].

Magnesium alloys have so many characteristics that would be useful in two dominant medical applications: biodegradable orthopedic implant materials and vascular stents [9–12]. Nevertheless, the main shortcomings of bioabsorbable magnesium alloy implants are their rapid degradation rate and seriously local alkalization, resulting in hydrogen evolution and loss of their original strength before bone tissues being healed [13]. Therefore, it is critical to for the degradation rate of the orthopedic implanted magnesium alloys to be controlled to match the bone healing rate.

Usually, manipulating the corrosion rate of biomedical magnesium alloys has three approaches: alloying, post-processing and surface modification [3,7,9–10]. Alloying of magnesium with Al, Zn, Mn, Ca, Li and RE (Y, Nd) elements shows an improvement in mechanical strength and corrosion resistance [7,14–15]. Mg–Li–Ca alloys as the potential biomaterials also attract other scientists' attention. Our prior studies [16–17] have designated that Mg–Li–Ca alloys possess outstanding corrosion resistance in comparison with Mg–Ca alloys. Moreover, post-processing such as extrusion and rolling can refine the microstructure, and thus enhance the strength and corrosion resistance of magnesium alloys [18]. Furthermore, surface modification is one of the key solutions and numerous modification methods have also been developed for improving the corrosion resistance of Mg alloy exposed to physiological environment [19–21]. Anodic oxidation [22–23], electro-deposition [24] and chemical conversion [25–26] as well as MAO/PLA coatings [27] are some popular technologies to produce a bioactive coating. The chemical conversion coating has been widely used due to their lower cost and easier operation.

To date, numerous investigations on Ca–P coatings, including β-tricalcium phosphate (β-TCP, β-$Ca_3(PO_4)_2$) [28–29], hydroxyapatite (HA) and Ca-deficient HA coatings [30–31] on magnesium alloys, have been made. Our previous study present that Ca–P coatings enhance the corrosion resistance of (AZ31 and Mg–1.0Ca) magnesium alloys [28–29]. It is demonstrated that Ca–P (β-TCP) coatings on AZ31 alloy show good adherence, proliferation and differentiation of MG63 cells [32]. And soaked in simulated body fluid, the hemolytic rates of AZ31B alloy with and without the Ca–P coating increase at the earlier stage of immersion and lower to an acceptable lower level over increasing immersion time. Also, the inflammation of the tissue around the AZ31B alloy implant could occur at the initial stage and would disappear for longer implantation, indicating that the biocompatibility of the alloy to the tissue could be improved after early implantation [33].

The Ca–P coating, composed of $CaHPO_4 \cdot 2H_2O$ layer with small amounts of Mg^{2+}, improves the surface cytocompatibility of magnesium significantly and provides magnesium with a remarkedly good surface bioactivity and promotes early bone growth at the implant/bone interface [34].

Up to now, zinc (Zn) phosphate conversion coatings on magnesium alloys were reported to enhancing corrosion resistance and biocompatibility [35–36]. Zn has been determined as a potential element for use in medical applications. Zn is a component of human bone and has been known to promote the growth of osteoblasts and has a basic safety for biomedical applications. The human body requirement for zinc is estimated to be 15 $mg \cdot day^{-1}$ [37]. Besides, the released zinc could be absorbed by the surrounding tissues and excreted through the gastrointestinal route and the kidney [37–38]. Therefore, it is proposed that the zinc release during degradation is safe. While calcium, as one of the major elements for human bones, is introduced in the Mg–Li alloy and the zinc phosphating solutions such that corrosion resistance of Mg–Li alloys is improved and the zinc phosphate conversion coating is refined [39].

In our previous study [39–41], the Zn–Ca–P coatings, successfully prepared on the surface of magnesium alloys (AZ31, AM50 and Mg–Li–Ca), have a flower-like morphology and homogenous fine grains, and have better

corrosion resistant than the substrate alloy. However, to the best of our knowledge, the blood compatibility of Zn–Ca–P conversion coating has not been systematically studied *in vitro* and *in vivo*.

In this paper, the microstructure and composition of the Zn–Ca–P coating were characterized. The corrosion behavior and bioactivity including the hemolysis test, the dynamic cruor time test, blood cell count and the platelet adhesion to membrane surface were also studied. It is expected that this work may help to confirm the blood biocompatibility *in vitro* of the Zn–Ca–P coating on the Mg–1.33Li–0.6Ca alloy and obtain a new surface modification method for degradable magnesium alloys.

2 Experimental

2.1 Materials

Pure Mg ingots were supplied by Guangling Magnesium Industry Science and Technology Co. Ltd., China. The Mg–1.33wt.%Li–0.6wt.%Ca ingots were fabricated by Institute of Metal Research, Chinese Academy of Sciences and extruded at Magnesium Industry in Chongqing Science and Technology Company, China. The material was cut into specimens of 20 mm × 20 mm × 4 mm, ground with 1500 grit SiC papers to ensure the same surface roughness. The samples were then cleaned ultrasonically in 100% ethanol, mild detergent and distilled water before drying and sterilization with ultraviolet.

The Zn–Ca–P coatings were prepared on the surface of the Mg–1.33Li–0.6Ca alloy in the phosphating baths at 55°C for 20 min. Calcium ions in the form of calcium nitrate were added into the zinc phosphate conversion solution leading to the formation of calcium modified zinc phosphate conversion (Zn–Ca–P) coatings. Fluoride ions were added as an activation agent. The pH value of the bath was adjusted to approximately 3.0 with phosphoric acid. The details can be found in our previous studies [39–41].

2.2 Microstructure characterization and composition

The surface morphologies of the Zn–Ca–P coating were discerned via a field-emission scanning electron microscope (Nova Nano SEM 450, USA). All samples for the scanning electron microscopy (SEM) observation were sputtered with gold. Energy dispersive X-ray spectrometer (EDS) attached to the SEM was used for elemental analysis.

2.3 *In vitro* degradation tests

The degradation behaviors of pure Mg, the Mg–1.33Li–0.6Ca alloys with and without the Zn–Ca–P coating were tested in Hank's balanced salt solution (HBSS), containing NaCl (8 $g \cdot L^{-1}$), KCl (0.4 $g \cdot L^{-1}$), $CaCl_2$ (0.14 $g \cdot L^{-1}$), $MgCl_2 \cdot 6H_2O$ (0.1 $g \cdot L^{-1}$), $NaHCO_3$ (0.35 $g \cdot L^{-1}$), $MgSO_4 \cdot 7H_2O$ (0.06 $g \cdot L^{-1}$), $Na_2HPO_4 \cdot 12H_2O$ (8 $g \cdot L^{-1}$), KH_2PO_4 (0.06 $g \cdot L^{-1}$) and glucose (1 $g \cdot L^{-1}$), buffered at pH 7.4 at a temperature of 36.5°C. The volume of hydrogen gas released during the immersion depended on the dissolution of magnesium. The pH value of HBSS was measured with 40 mL HBSS per cm^2 of exposed surface area over an immersion period of 120 h at 36.5°C. In the initial immersion of 10 h, the amount of hydrogen release and pH were recorded per hour. At the end of the test, final cleaning of the sample was carried out by dipping it into the solution (200 g Cr_2O_3, 10 g $AgNO_3$, 20 g $Ba(NO_3)_2$ and 1000 mL distilled water) for 5 min followed by washing with distilled water. The hydrogen evolution rate (HER) and weight loss rate were calculated according to the literature [34].

2.4 *In vitro* hemocompatibility evaluation test

In vitro hemocompatibility evaluation was identified by the hemolysis ratio measurement [42], dynamic blood-clotting tests [43], blood count, platelet adhesion and SEM observation [44–45].

2.4.1 Hemolysis test

Hemolysis tests were conducted according to the instruction of the ISO 10993-4: 2002 [46]. Extracting solution of material: The samples (with dimensions of 20 mm × 20 mm × 4 mm) were put into 25 mL beakers according to the ISO 10993-1 standard. The sample surface area/extraction medium volume equals 3 cm^2/mL. 10 mL saline was poured into the beakers, and then they were kept in a shaking bath at 36.5°C for 30 min, and centrifuged at a rate of 1500 r/min for 10 min, then supernatant is obtained.

Anticoagulant citrate dextrose (ACD) blood was supplied from the hospital attached to Shandong University of Science and Technology, China. Then, 0.2 mL diluted ACD whole blood (8 mL ACD whole blood was diluted by 10 mL normal saline) was dropped into the material extracting solution. Distilled water and normal saline were used as positive and negative controls, respectively. The absorbency of the solution was measured with a ultraviolet

spectrophotometer (UNIC-7200, China) at 545 nm. The hemolysis ratio (HR) can be derived from the equation as follows [47]:

$$\mathrm{HP}/\% = \frac{\mathrm{AS}-\mathrm{AN}}{\mathrm{AP}-\mathrm{AN}} \times 100 \quad (1)$$

where, AS is the absorbency of the samples; AP and AN denote the absorbencies of the positive control and the negative control, respectively.

2.4.2 Dynamic blood clotting test

Each sample was placed at the bottom of a 25 mL beaker; 0.1 mL ACD whole blood was dropped on the surface of the samples. The beakers containing the blood samples were kept in a thermostat at 36.5°C. The blood clotting test was carried out by spectrophotometric measurement of the absorbency of the blood samples (after 5, 20, 35, 50, 90 and 135 min) that had been diluted by 50 mL distilled water at 540 nm. For each sample, average optical density was obtained from three measurements.

2.4.3 Blood count

Blood count, including red blood cell (RBC), white blood cell (WBC) and platelets (PLT), was evaluated using the blood cell count method. Venous blood (3 mL) from a healthy volunteer was collected into a 25 mL beaker that contained 0.5 mL of sodium citrate (20 $g \cdot L^{-1}$) anticoagulant. Then, the pure Mg, Mg–1.33Li–0.6Ca alloy with and without the Zn–Ca–P coating samples were immediately immersed in the blood. The numbers of RBC, WBC and PLT were measured using an automatic hematology analyzer (Sysmex, XT-1800i, Japan) after the samples were immersed in blood for 30 min. Three parallel samples were evaluated in each group.

2.4.4 Platelet adhesion

Platelet rich plasma (PRP) was prepared by taking a sample of venous blood from a healthy volunteer. 9 mL of blood was mixed with 1 mL of 3.8% trisodium citrate, then centrifuged at a rate of 1000 r/min for 10 min. The pure Mg, Mg–1.33Li–0.6Ca alloys with and without Zn–Ca–P coating were soaked in PRP for 30 min at 36.5°C. The platelets in PRP were allowed to adhere and spread on the membrane surface; and non-adherent platelets were removed by washing the surface with phosphate buffer saline (PBS, pH 7.4) and mixed with 2.0% (w/v) glutaraldehyde solution. Then adherent platelets were dehydrated with each gradient immersion in 30%, 50%, 70%, 80%, 90% and 100% ethanol for 10 min in turn. These samples were later hydrated by critical point drying and sputtered with gold. Adhesion and deformation of platelets on blood contacting surface were evaluated with SEM.

2.5 Statistic analysis

Statistical analysis was performed with SPSS 16.0 (SPSS, Inc., Chicago, USA) to evaluate the differences in each group; all data were expressed as the mean ± SD. The experimental values were analyzed using the Student's *t*-test. The statistical significance was defined as $p < 0.05$.

3 Results and discussion

3.1 Morphology of the Zn–Ca–P coating

The SEM image of the Zn–Ca–P coating on the Mg–1.33Li–0.6Ca alloy is shown in Fig. 1(a). The crystalline Zn–Ca–P coating displays a flower-like morphology with micropores.

The EDS results of the Zn–Ca–P coating, shown in Fig. 1(b), demonstrate that the films are mainly composed of Mg, Zn, Ca, O, C and P, indicating the possible presence

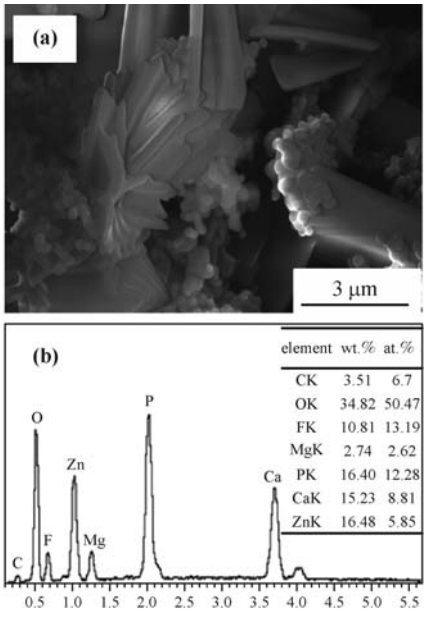

Fig. 1 **(a)** SEM image of the Zn–Ca–P coating on the Mg–1.33Li–0.6Ca alloy and **(b)** EDS results of the Zn–Ca–P coating composite.

of $Zn_3(PO_4)_2 \cdot 4H_2O$ and $CaZn_2(PO_4)_2$ [39–41]. The scenario implies that the Zn–Ca–P coating has been successfully coated on the surface of the Mg–1.33Li–0.6Ca alloy.

Our prior investigation designates that zinc is predominantly in the form of crystalline $Zn_3(PO_4)_2 \cdot 4H_2O$, a few Zn and ZnO. Moreover, the Zn–Ca–P coating has a much higher content of phosphor and Ca. The composition analysis of Zn–Ca–P coating mainly contains the hopeite crystals and possibly a few of $Ca_3(PO_4)_2$ [25]. The alkalization of the solution facilitates the precipitation of insoluble phosphates $Mg_3(PO_4)_2$, $Ca_3(PO_4)_2$ and $Zn_3(PO_4)_2$ [39].

3.2 Corrosion behavior

The immersion tests show that the average rates of weight loss of pure Mg, the Mg–1.33Li–0.6Ca alloys without and with the Zn–Ca–P coating are respectively 0.291, 0.064 and 0.041 $mg \cdot cm^{-2} \cdot day^{-1}$ after an immersion in Hank's solution for 120 h. The results indicate that the Zn–Ca–P coating improved the corrosion resistance of the Mg–1.33Li–0.6Ca alloy, superior to that of pure Mg.

Simultaneously, hydrogen generation was observed on the three sample surfaces during the period of immersion. Figure 2 presents the HER values of pure Mg, the Mg–1.33Li–0.6Ca alloys with and without Zn–Ca–P coating as a function of the immersion time. Obviously, the HER of pure Mg increased with immersion time, which is much faster than the Mg–1.33Li–0.6Ca alloy without and with Zn–Ca–P coating. The HER of the Mg–1.33Li–0.6Ca alloy descended slowly. In the first hour of soaking, corrosion products formed and covered on the corrosion pits and thus prevented the hydrogen releasing. Our previous investigation has demonstrated that filiform corrosion occurred due to the formation of corrosion product film [25,39,41]. Herein the HER of the Mg–1.33Li–0.6Ca alloy maintained at a stable level. It exhibits two stages in the curve of the HER of the Mg–1.33Li–0.6Ca alloy with the Zn–Ca–P coating over time in Hank's solution. The HER decreased rapidly in the initial stage of immersion, and then became more slowly than the Mg–1.33Li–0.6Ca alloy. Obviously, the average HER of the Mg–1.33Li–0.6Ca alloy with the Zn–Ca–P coating was the lowest. That is, it has the best corrosion resistance, which is consistent with the result of weight loss and our previous research results [39].

Figure 3 shows the changing trend of pH value of the solution, processing in three stages in the initial stage. Firstly, the pH values of three samples gradually increased from 7.8 to 8.2 after an immersion of 40 h in Hank's

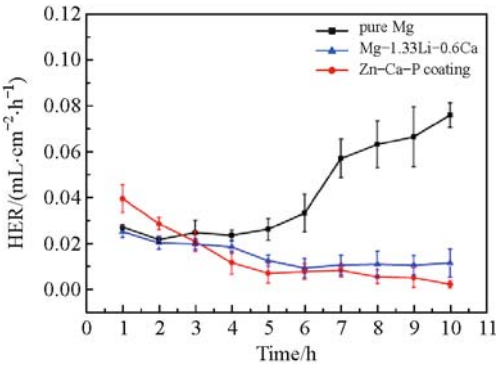

Fig. 2 Hydrogen evolution rates for pure Mg, the Mg–1.33Li–0.6Ca alloy and the Zn–Ca–P coating immersed for 10 h in Hank's solution.

solution. Secondly, the pH values, especially for the pure Mg sample and the Mg–1.33Li–0.6Ca alloy, increased rapidly. In the third stage, the pH values for the Mg–1.33Li–0.6Ca alloys with and without the Zn–Ca–P coating have a tendency to be stable, but that for pure Mg continues to rise. The consequence is in good accordance with the HER. The corrosion, occurring on the Mg–1.33Li–0.6Ca alloy, is ascribed to the micro-galvanic corrosion between the α-Mg matrix and the secondary phase Mg_2Ca in the microstructure. The Mg_2Ca particles have a relatively high potential and being the cathode, whereas the α-Mg matrix has a lower potential as the anode. The corrosion products of the Mg–1.33Li–0.6Ca alloy, predominately consisted of LiOH, $Mg(OH)_2$, $CaCO_3$, $MgCO_3$, $CaMg(CO_3)_2$ and $CaMgPO_4$ in Hank's solution, could completely cover the alloy surface and form a dense and protective layer [39]. On the contrary, the loose corrosion products of pure Mg, composed of $Mg(OH)_2$ and trace of HA, could hardly offer efficient protection, particularly in chloride solution due to the solution of $Mg(OH)_2$ into soluble $MgCl_2$ [48].

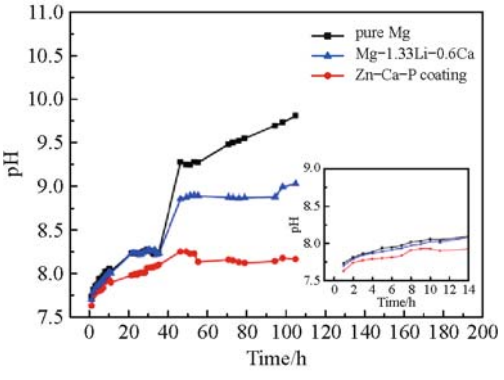

Fig. 3 The pH values for pure Mg, the Mg–1.33Li–0.6Ca alloy and the Zn–Ca–P coating immersed for 120 h in Hank's solution.

Interestingly, the crystalline Zn–Ca–P coating has a highest corrosion rate in the initial period of immersion, which is attributable to the micro-pores (Fig. 1) existed in the coating such that the solution penetrated into the coating, and thus led to a galvanic corrosion between the coating and the substrate. After that, the protective corrosion products gradually deposited and sealed on the pores resulted in the decrease in corrosion rate.

3.3 Hemocompatibility of the coated alloy

HR is a convenient and easily observable indicator of RBC damage that can occur during the sample contacting with blood. It signifies RBC membrane damage and the consequent release of hemoglobin into the surrounding medium [49]. HR is regarded as a common screening test, especially for medical materials in contact with blood directly. The lyses of RBC with the release of hemoglobin cause a high hemoglobin level, normally indicating hemolysis. The hemolysis is, to some extent, acceptable, while a higher degree of hemolysis indicates a higher risk of RBC broken occurring on the material surface.

Figures 4 and 5 show the absorbency and the HR values of pure Mg, Mg–1.33Li–0.6Ca alloys with and without the Zn–Ca–P coating. The HR values of pure Mg and the Mg–1.33Li–0.6Ca alloy are higher than 5%. However the HR value of the Zn–Ca–P coating is 4.47%, lower than 5%, conforming to the accepted HR value of biomaterials for medical application. Obviously, the result indicates that the hemolysis of the Mg–1.33Li–0.6Ca alloy decreased after being coated by Zn–Ca–P.

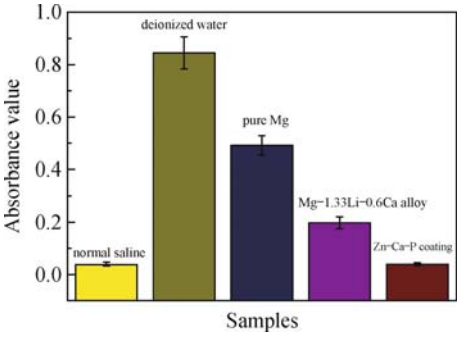

Fig. 4 Absorbance values for pure Mg, the Mg–1.33Li–0.6Ca alloy and the Zn–Ca–P coating.

A considerable number of studies [47,50–51] show that the HRs of different magnesium alloys are much higher than 5%, which may be ascribed to the fact that normal saline is chosen as the extract. Because the high concentration of Cl^- in normal saline causes serious corrosive reaction with magnesium, the osmotic pressure and pH value reaches a higher level, which could be the main reason for the high hemolysis ratio of pure Mg and the Mg–1.33Li–0.6Ca alloy. Just as the Zn–Ca–P coating can effectively slow down the degradation of the Mg–1.33Li–0.6Ca alloy, the hemolysis of the alloy is thus reduced. The Zn–Ca–P coating can make an enhancement in biocompatibility for the Mg–1.33Li–0.6Ca alloy at least at the early stage of implantation.

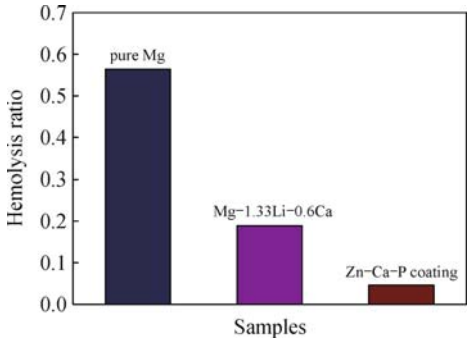

Fig. 5 Hemolysis ratios for pure Mg, the Mg–1.33Li–0.6Ca alloy and the Zn–Ca–P coating.

3.4 Blood count

Blood cell count is a kind of method to evaluate the biocompatibility of biomedical materials *in vitro*. The influence of blood cells for pure Mg, the Mg–1.33Li–0.6Ca alloy without and with the Zn–Ca–P coating samples is shown in Fig. 6. There are reductions in PLT, RBC and WBC after immersion in blood for 30 min *in vitro*. This change is more obvious in the Mg–1.33Li–0.6Ca alloy than the Zn–Ca–P coating (shown in Fig. 7), and the statistical significance corresponds to no difference ($p > 0.05$). That is, pure Mg, the Mg–1.33Li–0.6Ca alloy and the Zn–Ca–P coating had no obvious destruction on blood cells *in vitro*, which has good blood compatibility.

3.5 Dynamic blood-clotting tests and platelet adhesion

In vitro dynamic blood-clotting time (DCT) reflects the degree of blood clotting with the increase in blood-sample contacting time. The DCT curves (Fig. 8) of pure Mg, the Mg–1.33Li–0.6Ca alloy and the Zn–Ca–P coating slow down with increasing in the blood-sample contacting time. As is shown, the absorbance values of such three samples decrease in the first 35 min and then the values for the Mg–1.33Li–0.6Ca alloy and the Zn–Ca–P coating sustain a

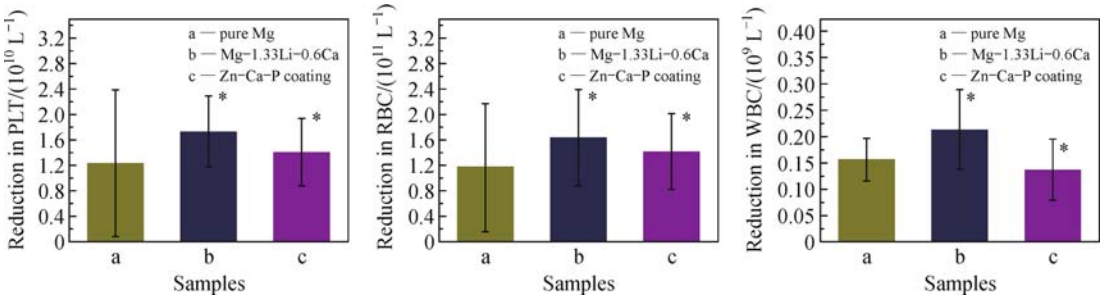

Fig. 6 Comparison of reduction of blood cells on the surfaces of pure Mg (a), the Mg–1.33Li–0.6Ca alloy (b) and the Zn–Ca–P coating (c) samples (*$p > 0.05$).

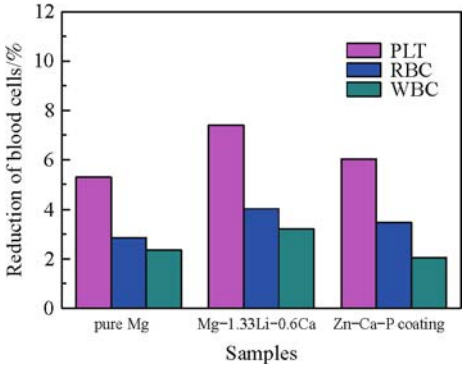

Fig. 7 Reduction of blood cells on the surfaces of pure Mg, the Mg–1.33Li–0.6Ca alloy and the Zn–Ca–P coating samples (% of initial blood cells).

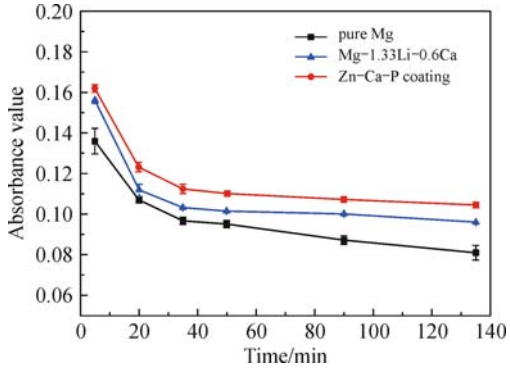

Fig. 8 Dynamic clotting time curves of pure Mg, the Mg–1.33Li–0.6Ca alloy and the Zn–Ca–P coating.

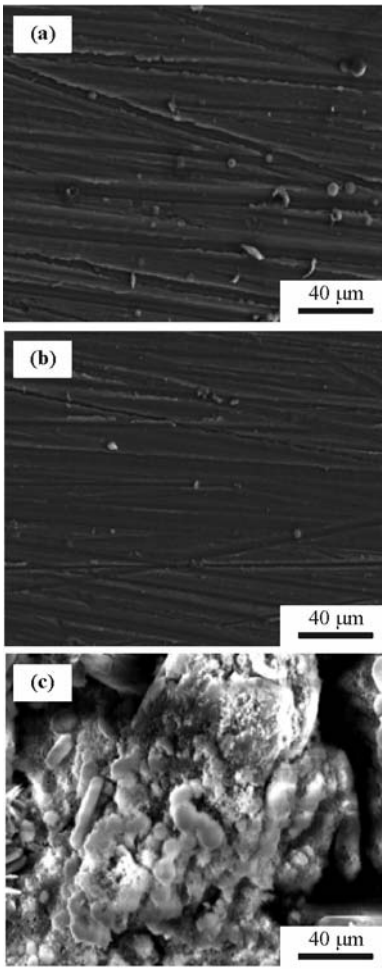

Fig. 9 SEM images of blood platelets adhesion on **(a)** pure Mg, **(b)** the Mg–1.33Li–0.6Ca alloy and **(c)** the Zn–Ca–P coating.

stable level for a long time, while that of the pure Mg continuously descends. All these indicate that such three samples have no obvious impact on the coagulation. On the whole, the absorbance value of the Zn–Ca–P coating is slightly higher than those of other samples, meaning that the Zn–Ca–P coating is superior to pure Mg and the Mg–1.33Li–0.6Ca alloy for reducing the cruor.

Figure 9 illustrates morphologies of human platelets adhering to pure Mg, the Mg–1.33Li–0.6Ca alloy and the Zn–Ca–P coating after incubation in PRP for 30 min. It can be seen that platelets keep the shape of round on the surfaces of the three samples, without any sign of pseudopodia-like structures. For platelet adhesion, all of the experimental samples presented negative activation.

4 Conclusions

1) The Zn–Ca–P coating has a flower-like crystalline morphology. Both of the Mg–1.33Li–0.6Ca alloy and the Zn–Ca–P coating are corrosion-resistant than pure Mg. The Zn–Ca–P coating on the Mg–1.33Li–0.6Ca alloy can reduce corrosion more significantly.

2) The Zn–Ca–P coating on the Mg–1.33Li–0.6Ca alloy reduces hemolysis percentage lower than 5% and has no obvious influence on blood cells, showing an excellent anticoagulant properties.

The Zn–Ca–P coating as a novel coating on the Mg–1.33Li–0.6Ca alloy may be found a promising biocompatible application in orthopaedic and cardiovascular fields. Further investigations will be assessed the cytotoxicity to assess its applicability as a long-term biocompatible coating, as well as its suitability as a corrosion protective coating for biodegradable metallic implants.

Acknowledgements This work was supported by the National Natural Science Foundation of China (Grant No. 51571134) and SDUST Research Fund (2014TDJH104). Thanks also go to Prof. Rongshi Chen for the alloy fabrication in Institute of Metal Research, Chinese Academy of Sciences and Ms. Xin-Xin Sun for the coating preparation in Shandong University of Science and Technology.

References

[1] Bostman O, Pihlajamaki H. Clinical biocompatibility of biodegradable orthopaedic implants for internal fixation: a review. Biomaterials, 2000, 21(24): 2615–2621

[2] Reifenrath J, Krause A, Bormann D, et al. A profound difference in the *in-vivo*-degradation and biocompatibility of two very similar rare-earth containing Mg-alloys in a rabbit model. Materialwissenschaft und Werkstofftechnik, 2010, 41: 1054–1061

[3] Zheng Y F, Gu X N, Witte F. Biodegradable metals. Materials Science and Engineering R: Reports, 2014, 77(2): 1–34

[4] Huehnerschulte T A, Angrisani N, Rittershaus D, et al. *In vivo* corrosion of two novel magnesium alloys ZEK100 and AX30 and their mechanical suitability as biodegradable implants. Materials, 2011, 4(6): 1144–1167

[5] Williams D. New interests in magnesium. Medical Device Technology, 2006, 17(3): 9–10

[6] Vormann J. Magnesium: nutrition and metabolism. Molecular Aspects of Medicine, 2003, 24(1–3): 27–37

[7] Zeng R C, Dietzel W, Witte F, et al. Progress and challenge for magnesium alloys as biomaterials. Advanced Engineering Materials, 2008, 10(8): B3–B14

[8] Sherriff J. Modern nutrition in health and disease. Australian Journal of Nutrition and Dietetics, 2000, 57(1): 55–56

[9] Staiger M P, Pietak A M, Huadmai J, et al. Magnesium and its alloys as orthopedic biomaterials: a review. Biomaterials, 2006, 27 (9): 1728–1734

[10] Witte F, Fischer J, Nellesen J, et al. *In vitro* and *in vivo* corrosion measurements of magnesium alloys. Biomaterials, 2006, 27(7): 1013–1018

[11] Zartner P, Cesnjevar R, Singer H, et al. First successful implantation of a biodegradable metal stent into the left pulmonary artery of a preterm baby. Catheterization and Cardiovascular Interventions, 2005, 66(4): 590–594

[12] Hermawan H, Dube D, Mantovani D. Developments in metallic biodegradable stents. Acta Biomaterialia, 2010, 6(5): 1693–1697

[13] Witte F, Kaese V, Switzer H, et al. *In vivo* corrosion of four magnesium alloys and the associated bone response. Biomaterials, 2005, 26(17): 3557–3563

[14] Zeng R C, Wang L, Zhang D F, et al. *In vitro* corrosion of Mg–6Zn–1Mn–4Sn–1.5Nd/0.5Y alloys. Frontiers of Materials Science, 2014, 8(3): 230–243

[15] Zhou W R, Zheng Y F, Leeflang M A, et al. Mechanical property, biocorrosion and *in vitro* biocompatibility evaluations of Mg–Li–(Al)–(RE) alloys for future cardiovascular stent application. Acta Biomaterialia, 2013, 9(10): 8488–8498

[16] Zeng R C, Sun L, Zheng Y F, et al. Corrosion and characterization of dual phase Mg–Li–Ca alloy in Hank's solution: The influence of microstructural features. Corrosion Science, 2014, 79: 69–82

[17] Zeng R C, Guo X L, Liu C L, et al. Study on corrosion of medical Mg–Ca and Mg–Li–Ca alloy. Acta Metallurgica Sinica - Chinese Edition, 2011, 47(11): 1477–1482 (in Chinese)

[18] Zhu S J, Liu Q, Qian Y F, et al. Mechanical property and corrosion behavior in simulated body fluid of Mg–Zn–Y–Nd alloy for cardiovascular stent application. Frontiers of Materials Science, 2014, 8(3): 256–263

[19] Zomorodian A, Brusciotti F, Fernandes A, et al. Anti-corrosion performance of a new silane coating for corrosion protection of AZ31 magnesium alloy in Hank's solution. Surface and Coatings Technology, 2012, 206(21): 4368–4375

[20] Abdal-hay A, Barakat N A M, Lim J K. Hydroxyapatite-doped poly(lactic acid) porous film coating for enhanced bioactivity and corrosion behavior of AZ31 Mg alloy for orthopedic applications. Ceramics International, 2013, 39(1): 183–195

[21] Zomorodian A, Garcia M P, Moura T, et al. Corrosion resistance of a composite polymeric coating applied on biodegradable AZ31 magnesium alloy. Acta Biomaterialia, 2013, 9(10): 8660–8670

[22] Gu X N, Li N, Zhou W R, et al. Corrosion resistance and surface biocompatibility of a microarc oxidation coating on a Mg–Ca alloy. Acta Biomaterialia, 2010, 7(4): 1880–1889

[23] Gao J H, Shi X Y, Yang B, et al. Fabrication and characterization

of bioactive composite coatings on Mg–Zn–Ca alloy by MAO/sol-gel. Journal of Materials Science: Materials in Medicine, 2011, 22 (7): 1681–1687

[24] Boccaccini A R, Keim S, Ma R, et al. Electrophoretic deposition of biomaterials. Journal of the Royal Society Interface, 2010, 7 (Suppl 5): S581–S613

[25] Zeng R C, Lan Z D, Kong L H, et al. Characterization of calcium-modified zinc phosphate conversion coatings and their influences on corrosion resistance of AZ31 alloy. Surface and Coatings Technology, 2011, 205(11): 3347–3355

[26] Lan W, Sun J C, Zhou A R, et al. Structures of zinc–manganese phosphate film and organic coating on magnesium alloys. Materials Science Forum, 2009, 610–613: 880–883

[27] Zeng R C, Qi W C, Song Y W, et al. *In vitro* degradation of MAO/PLA coating on Mg–1.21Li–1.12Ca–1.0Y alloy. Frontiers of Materials Science, 2014, 8(4): 343–353

[28] Zhang C Y, Zeng R C, Liu C L, et al. Preparation of calcium phosphate coatings on Mg–1.0Ca alloy. Transactions of Nonferrous Metals Society of China, 2010, 20: s655–s659

[29] Zhang C Y, Zeng R C, Liu C L, et al. Comparison of calcium phosphate coatings on Mg–Al and Mg–Ca alloys and their corrosion behavior in Hank's solution. Surface and Coatings Technology, 2010, 204(21–22): 3636–3640

[30] Wen C L, Guan S K, Peng L, et al. Characterization and degradation behavior of AZ31 alloy surface modified by bone-like hydroxyapatite for implant applications. Applied Surface Science, 2009, 255(13–14): 6433–6438

[31] Wang H X, Guan S K, Wang X, et al. *In vitro* degradation and mechanical integrity of Mg–Zn–Ca alloy coated with Ca-deficient hydroxyapatite by the pulse electrodeposition process. Acta Biomaterialia, 2010, 6(5): 1743–1748

[32] Tan L L, Wang Q, Geng F, et al. Preparation and characterization of Ca–P coating on AZ31 magnesium alloy. Transactions of Nonferrous Metals Society of China, 2010, 20: s648–s654

[33] Wang Q, Tan L L, Xu W L, et al. Dynamic behaviors of a Ca–P coated AZ31B magnesium alloy during *in vitro* and *in vivo* degradations. Materials Science and Engineering B, 2011, 176 (20): 1718–1726

[34] Xu L P, Pan F, Yu G N, et al. *In vitro* and *in vivo* evaluation of the surface bioactivity of a calcium phosphate coated magnesium alloy. Biomaterials, 2009, 30(8): 1512–1523

[35] Zhang S X, Li J A, Song Y, et al. *In vitro* degradation hemolysis and MC3T3-E1 cell adhesion of biodegradable Mg–Zn alloy. Materials Science and Engineering C, 2009, 29(6): 1907–2005

[36] Zhang S X, Zhang X N, Zhao C L, et al. Research on an Mg–Zn alloy as a degradable biomaterial. Acta Biomaterialia, 2010, 6(2): 626–640

[37] Tapiero H, Tew K D. Trace elements in human physiology and pathology: zinc and metallothioneins. Biomedicine and Pharmacotherapy, 2003, 57(9): 399–411

[38] Stulikova I, Smola B. Mechanical properties and phase composition of potential biodegradable Mg–Zn–Mn-base alloys with addition of rare earth elements. Materials Characterization, 2010, 61(10): 952–958

[39] Zeng R C, Sun X X, Song Y W, et al. Influence of solution temperature on corrosion resistance of Zn–Ca phosphate conversion coating on biomedical Mg–Li–Ca alloys. Transactions of Nonferrous Metals Society of China, 2013, 23(11): 3293–3299

[40] Zeng R C, Lan Z D. Influence of bath temperature of conversion treatment process on corrosion resistance of zinc calcium phosphate conversion film on AZ31 magnesium alloy. The Chinese Journal of Nonferrous Metals, 2010, 20: 1461–1466

[41] Zeng R C, Zhang F, Lan Z D, et al. Corrosion resistance of calcium-modified zinc phosphate conversion coatings on magnesium–aluminium alloys. Corrosion Science, 2014, 88(6): 452–459

[42] Acker J P, Croteau I M, Yi Q L. An analysis of the bias in red blood cell hemolysis measurement using several analytical approaches. Clinica Chimica Acta, 2012, 413(21–22): 1746–1752

[43] Huang J, Dong P, Hao W C, et al. Biocompatibility of TiO_2 and TiO_2/heparin coatings on NiTi alloy. Applied Surface Science, 2014, 313: 172–182

[44] Zhou C R, Yi Z J. Blood-compatibility of polyurethane/liquid crystal composite membranes. Biomaterials, 1999, 20(22): 2093–2099

[45] Dong Y X, Chen Y S, Chen Q, et al. Characterization and blood compatibility of TiC_xN_{1-x} hard coating prepared by plasma electrolytic carbonitriding. Surface and Coatings Technology, 2007, 201(21): 8789–8795

[46] ISO/DIS 10993-4. Biological evaluation of medical devices - Part 4: Selection of tests for interactions with blood, 2006

[47] Zhen Z, Xi T F, Zheng Y F, et al. *In vitro* study on Mg–Sn–Mn alloy as biodegradable metals. Materials Science and Technology, 2014, 30(7): 675–685

[48] Wang Y, Wei M, Gao J C, et al. Corrosion process of pure magnesium in simulated body fluid. Materials Letters, 2008, 62 (14): 2181–2184

[49] Hess J R, Sparrow R L. Red blood cell hemolysis during blood bank storage: using national quality management data to answer basic scientific questions. Transfusion, 2009, 49(12): 2599–2603

[50] Gu X N, Zheng Y F, Cheng Y, et al. *In vitro* corrosion and biocompatibility of binary magnesium alloys. Biomaterials, 2009, 30(4): 484–498

[51] Zhang E L, Yin D S, Xu L P, et al. Microstructure, mechanical and corrosion properties and biocompatibility of Mg–Zn–Mn alloys for biomedical application. Materials Science and Engineering C, 2009, 29(3): 987–993